Since January 2020 Elsevier has created a COVID-19 resource centre with free information in English and Mandarin on the novel coronavirus COVID-19. The COVID-19 resource centre is hosted on Elsevier Connect, the company's public news and information website.

Chemosphere 306 (2022) 135578

Contents lists available at ScienceDirect

Chemosphere

journal homepage: www.elsevier.com/locate/chemosphere

CaZnO-based nanoghosts for the detection of ssDNA, pCRISPR and recombinant SARS-CoV-2 spike antigen and targeted delivery of doxorubicin

Navid Rabiee [a,b,c,**], Omid Akhavan [a], Yousef Fatahi [d,e], Amir Mohammad Ghadiri [f], Mahsa Kiani [f], Pooyan Makvandi [g], Mohammad Rabiee [h], Mohammad Hossein Nicknam [i,j], Mohammad Reza Saeb [k], Rajender S. Varma [l], Milad Ashrafizadeh [m], Ehsan Nazarzadeh Zare [n], Esmaeel Sharifi [o], Eder C. Lima [p,*]

[a] Department of Physics, Sharif University of Technology, P.O. Box 11155-9161, Tehran, Iran
[b] School of Engineering, Macquarie University, Sydney, New South Wales, 2109, Australia
[c] Department of Materials Science and Engineering, Pohang University of Science and Technology (POSTECH), 77 Cheongam-ro, Nam-gu, Pohang, Gyeongbuk, 37673, South Korea
[d] Department of Pharmaceutical Nanotechnology, Faculty of Pharmacy, Tehran University of Medical Sciences, Tehran, Iran
[e] Nanotechnology Research Centre, Faculty of Pharmacy, Tehran University of Medical Sciences, Tehran, Iran
[f] Department of Chemistry, Sharif University of Technology, Tehran, Iran
[g] Istituto Italiano di Tecnologia, Centre for Materials Interfaces, Viale Rinaldo Piaggio 34, 56025, Pontedera, Pisa, Italy
[h] Biomaterial Group, Department of Biomedical Engineering, Amirkabir University of Technology, Tehran, Iran
[i] Molecular Immunology Research Center, Tehran University of Medical Sciences, Tehran, Iran
[j] Department of Immunology, School of Medicine, Tehran University of Medical Sciences, Tehran, Iran
[k] Department of Polymer Technology, Faculty of Chemistry, Gdánsk University of Technology, G. Narutowicza 11/12, 80-233, Gdánsk, Poland
[l] Regional Centre of Advanced Technologies and Materials, Czech Advanced Technology and Research Institute, Palacky University, Šlechtitelů 27, 783 71, Olomouc, Czech Republic
[m] Faculty of Engineering and Natural Sciences, Sabanci University, Orta Mahalle, Üniversite Caddesi No. 27, Orhanlı, Tuzla, 34956, Istanbul, Turkey
[n] School of Chemistry, Damghan University, Damghan, 36716-41167, Iran
[o] Department of Tissue Engineering and Biomaterials, School of Advanced Medical Sciences and Technologies, Hamadan University of Medical Sciences, 6517838736, Hamadan, Iran
[p] Institute of Chemistry, Federal University of Rio Grande Do Sul (UFRGS), Porto Alegre, RS, Brazil

HIGHLIGHTS

- The first inorganic-based nanoghosts with a similar performance same as the MSCs.
- Highly sensitive to ssDNA, pCRISPR, and SARS-CoV-2.
- Highly selective to SARS-CoV-2 in different environments.
- Innovative, green, and cost-effective method to prepare an optical nano-probe for the SARS-CoV-2 detection.

GRAPHICAL ABSTRACT

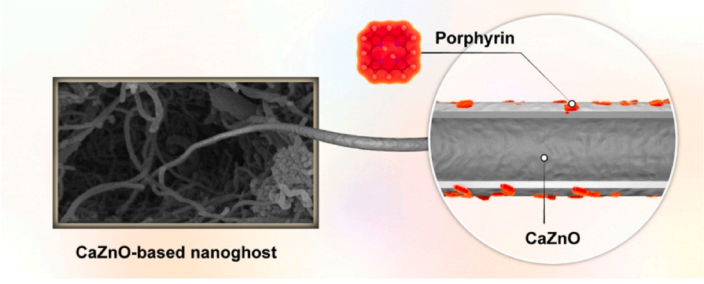

* Corresponding author.
** Corresponding author. Department of Physics, Sharif University of Technology, P.O. Box 11155-9161, Tehran, Iran.
E-mail addresses: nrabiee94@gmail.com (N. Rabiee), profederlima@gmail.com, eder.lima@ufrgs.br (E.C. Lima).

https://doi.org/10.1016/j.chemosphere.2022.135578
Received 10 February 2022; Received in revised form 23 June 2022; Accepted 29 June 2022
Available online 4 July 2022

ARTICLE INFO

Handling Editor: Hassan Karimi-Maleh

Keywords:
Nanoghosts
ssDNA
pCRISPR
Gene delivery
In-situ biosensor
SARS-CoV-2

ABSTRACT

Overexpression of proteins/antigens and other gene-related sequences in the bodies could lead to significant mutations and refractory diseases. Detection and identification of assorted trace concentrations of such proteins/antigens and/or gene-related sequences remain challenging, affecting different pathogens and making viruses stronger. Correspondingly, coronavirus (SARS-CoV-2) mutations/alterations and spread could lead to over-expression of ssDNA and the related antigens in the population and brisk activity in gene-editing technologies in the treatment/detection may lead to the presence of pCRISPR in the blood. Therefore, the detection and evaluation of their trace concentrations are of critical importance. CaZnO-based nanoghosts (NGs) were synthesized with the assistance of a high-gravity technique at a 1,800 MHz field, capitalizing on the use of *Rosmarinus officinalis* leaf extract as the templating agent. A complete chemical, physical and biological investigation revealed that the synthesized NGs presented similar morphological features to the mesenchymal stem cells (MSCs), resulting in excellent biocompatibility, interaction with ssDNA- and/or pCRISPR-surface, through various chemical and physical mechanisms. This comprise the unprecedented synthesis of a fully inorganic nanostructure with behavior that is similar to MSCs. Furthermore, the endowed exceptional ability of inorganic NGs for detective sensing/folding of ssDNA and pCRISPR and recombinant SARS-CoV-2 spike antigen (RSCSA), along with *in-situ* hydrogen peroxide detection on the HEK-293 and HeLa cell lines, was discerned. On average, they displayed a high drug loading capacity of 55%, and the acceptable internalizations inside the HT-29 cell lines affirmed the anticipated MSCs-like behavior of these inorganic-NGs.

1. Introduction

The convergence between chemistry, nanoscience, and biotechnology leads to the developing of new methods/technologies for advanced creations (Akça et al., 2021; Karaman, 2021, 2022; Deng et al., 2022). These technologies are based on the innovative findings of the scientists based on their fundamental knowledge; however, sometimes, these innovative findings lead to unwanted effects with negative impacts (Liu et al., 2022; Nosrati et al., 2022; Shokri et al., 2022). One of the unwanted effects with negative implications on biomedical engineering science is the cytotoxicity of the developed new (nano)materials. In this case, several research groups were focused on reducing the cytotoxicity, but the mechanism of this cytotoxicity is what ought to be addressed (Huang et al., 2021; Saadati et al., 2021; Seidi et al., 2021). Nanoghosts (NGs) (Toledano Furman et al., 2013; Krishnamurthy et al., 2016) are novel and promising alternatives to targeted delivery systems, which are grounded based on the reconstruction of the human bone marrow-derived mesenchymal stem cells (MSCs) cytoplasmic membranes (Akhavan et al., 2013b), mainly for tumor sites targeting (Brown, 2013; Kaneti et al., 2016). The concept of MSCs-based nano-carriers is of great importance in view of the chemistry and morphology lenses. In these carriers, the 'ghost' cells are prepared by removing organelles and cytoplasm of MSC, with the NGs size of ~200 nm. The outstanding feature is their extraordinary biocompatibility and their considerable loading capacity compared to the other vesicle-derived types of carriers (Lupu-Haber et al., 2019; Hwang et al., 2020). However, since paramount problems are mainly because by the genetic alterations and restructured natural organs, the use of such cellular-derived compounds could cause secondary health risks to humans and the environment in the not-too-distant future. For this reason, an inspirational approach may exploit the characteristics of cells and natural organs −, the mission of synthetic precursors with multifunctional features (Mitra et al., 2017; Teplensky et al., 2017). Also, this is an important factor in developing the (nano)structures with fully modifiable features; therefore, mimicking the structures of the NGs in the laboratory is considered one of the priorities for the next generation of translational medicine.

The art of selective morphological synthesis is a specialty in advanced chemistry (Akhavan, 2010; Akhavan et al., 2016b; Ahmadi et al., 2020; Kiani et al., 2020b), wherein the inspiration from nature may provide discerning morphological syntheses, as most of the surface and bulk properties of these nano-carriers can be imitated (Kholafazad-Kordasht et al., 2021; Kordasht et al., 2021; Mobed et al., 2021; Sardaremelli et al., 2021). The noticeable primary feature of NGs is their hollow bulk structure; the structure of the empty space experiences more than 80% of the bulk. Thus, structures with high and regular porosity could be a good candidate to imitate the bulk morphology of NGs. On the other hand, for their significant biocompatibility, the successful and relatively strong superficial interactions of these NGs with animal/human cells are not principally guest-host grounded. In order to attain such interactive mimicry, lipid receptors or structures are additionally needed, but that option dramatically increases the cost of preparation, thus limiting the commercialization of such nano-carriers.

Despite extensive research on this class of synthetic vesicle-derived membranes, no applicable and systematic protocol exists to compete with naturally extracted NGs. Also, there have been no attempts made to design and synthesize fully inorganic nanostructure with the behavior similar to MSCs, rendering the deployment of NGs and MSCs very critical. It should be noted that inorganic nanostructures are considered the next-gold standard materials due to their significant stability, tunable surface, bulk structure, and modifiable features. Therefore, replacing the most precious biological-based materials, including the MSCs, with fully inorganic NGs is of great importance.

In a serendipitous manner and prompted by our prior experience, we realized an unprecedented synthesis of a synthetic NG based on calcium and zinc by deploying the high gravity technique. The primary aim of this study was to use calcium- and zinc-based nanostructures for smart therapeutics/gene delivery applications and sensing abilities. However, after random morphological investigations, we envisioned that the present material could be the first inorganic NG synthesized in the laboratory. Therefore, a variety of physical, chemical, and biological measurements were deployed to characterize the synthesized inorganic NG (Scheme 1) to optimize smart cargo delivery applications and biosensing abilities. Additionally, the synthesized NGs were assessed to develop very light, inexpensive, and practical nanobiosensors.

2. Materials and methods

2.1. Synthesis of CaZnO-based NGs

In order to achieve highly stable, mono-dispersed CaZnO-based NGs with a reduced time of reaction and the reduced temperature, the modified rotating packed bed (RPB) system was used based on our previous explorations (Ghadiri et al., 2020; Rabiee et al., 2020a, 2021c; Rabiee et al., 2020f; Bagherzadeh et al., 2021). In this approach, 1:4 stoichiometric amounts of calcium chloride hexahydrate and the zinc acetate di-hydrate were reacted together and then poured into the internal space of the modified RPB system. Next, the extracted solution (20 mL) from the leaves of *Rosmarinus officinalis* in the water/ethanol

(1:1) was added to the reaction space.

Based on our previous know-how (Rabiee et al., 2021a, 2021b), the higher rotation of the internal circulation space leads to decreased temperature and time of reaction but optimizing the rotation speed is of great importance. In this experiment, 1400 rpm was selected as the optimized rotation speed, which steers to the high-gravity factor equal to 182. The temperature is the other crucial parameter that needs to be optimized. The aim of using the RPB system is to deploy lower temperatures.

Due to the unprecedented nature of the synthesis of this type of nanomaterial, therefore, there is no scale available as guidance to compare the optimized temperature. Thus, the morphology of the synthesized CaZnO-based NGs is the yardstick for optimizing the physical and chemical parameters. After several explorations, the temperature of 165 °C was applied in this context. Notably, before any reaction on the internal space of the RPB, the space should be degassed with a flow of oxygen for an hour.

2.2. Nanomaterial fabrication for biosensor assay

An amount of 6 mg of as-prepared tetramesitylporphyrin (H_2TMP) was fully dispersed into 15 mL of DMF, and the slurry was treated with ultrasonic in the dark for 30 min. Subsequently, 10 mg of CaZnO NG was introduced into the reactional mixture to produce an adequate nanomaterial for biosensor assay. Finally, the reactional mixture was magnetically stirred for 24 h in a dark place at ambient temperature.

2.3. Cell evaluations

This is an important step in providing repeatable cell evaluation experiments to make the study suitable for pre-clinical and industrial applications. In addition, all the samples should be sterilized by using ultraviolet exposure before any cellular and molecules studies. In this study, the cytocompatibility investigations were conducted using the MTT (3-[4,5-dimethylthiazol-2-yl]-2,5-diphenyltetrazolium bromide) assay at 24 and 48 h.

In order to evaluate a complete cellular experiment, four different cell lines of HEK-293 (ATCC CRL-1721™), PC12 (ATCC CRL-1721™), HepG2 (ATCC HB 8065), and HeLa (ATCC CCL-2) were applied for a full investigation. In each well, 1×10^5 cells were cultured with assistance from Dulbecco's Modified Eagle's Medium, which included 100 IU/mL streptomycin, 10% fetal bovine serum, and 100 IU/mL penicillin, were incubated at 37 °C at 5% CO_2. After completing each time point, the MTT solution (100 μL, 5 mg/mL in PBS) was added to each well, followed by further incubations and removal of the medium; ensued, formazan precipitates were dissolved in DMSO. The results were evaluated by Elisa reader (ELX808, BioTek) at 570 nm.

2.4. Investigation of the ssDNA and NGs interactions

An aliquot of 55 μL of the NGs-porphyrin at 5 g/L and 24 μL of DNA were incubated for 20 min at 37 °C to analyze the possible interaction between the ssDNA and synthesized NGs. Also, the host-guest molecules were prepared using different concentrations. Then, these complexes were centrifuged at 14,000 rpm for 10 min for purification. The precipitates were further dissolved in ultrapure water and washed with ultrapure water in abundance.

2.5. pCRISPR and ssDNA biosensor assay

In order to investigate the biosensor assay of the pCRISPR and ssDNA, two different cell lines of PC12 and HEK-293 were cultured under the aforementioned conditions. The cells/well population was adjusted the same as the cytocompatibility experiments. After a day (24 h), the release of the hydrogen peroxide was investigated based on the oxidation of the porphyrin (degradation of the porphyrin) upon the hydrogen peroxide release.

2.6. Synthesis of NGs in assistance of radiofrequency

The same device of RPB was used for the synthesis in this step, with some modifications. In this case, the RPB system was coupled with an sXc1800 exposure unit (Zurich, Switzerland) (Schuderer et al., 2004; Gerner et al., 2010). This device has two completely different waveguides that enables to apply different RF exposures. In addition, it is equipped to modulate GSM 1800 MHz fields in a sinus manner. All of the other conditions remained unchanged.

2.7. Optical detection of recombinant SARS-CoV-2 spike antigen

The targeted antigen, SARS-CoV-2 spike antigen, was diluted serially with varying concentrations ranging from 10 to 1000 ng/mL and appropriate concentrations (different ratios of the nano-probe and the RSCSA of the prepared modified NGs added to the solutions. The solutions were incubated for 15 min at room temperature, and the fluorescent spectroscopy examined the color change to evaluate the RSCSA concentration.

3. Results and discussion

The original inorganic NG, CaZnO blended with *Rosmarinus officinalis*, was characterized using different analytical techniques such as transmission electron microscopy (TEM; ZEISS) and field-emission scanning-electron-spectroscopy (FESEM; Mira-3 TESCAN), atomic force microscopy (AFM), and x-ray diffraction (XRD) (Fig. 1).

These CaZnO NGs displayed an array of inorganic nanosystems with a predictable sequence based on the morphological analysis. A little

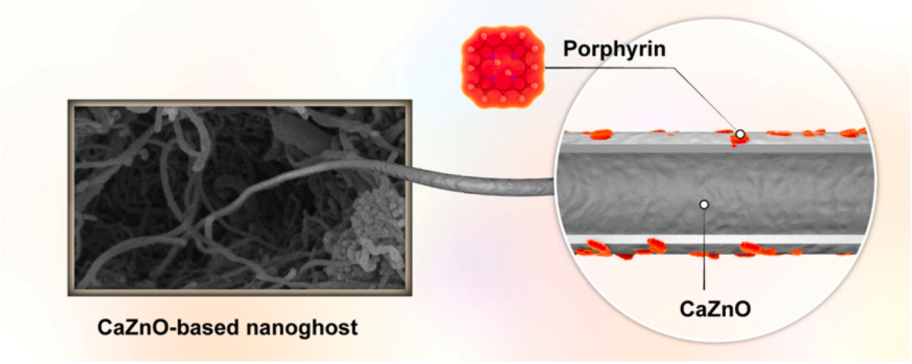

Scheme 1. Schematic illustration of the synthesized CaZnO-based NGs and their porphyrin-adorned surface for biosensor and drug delivery applications.

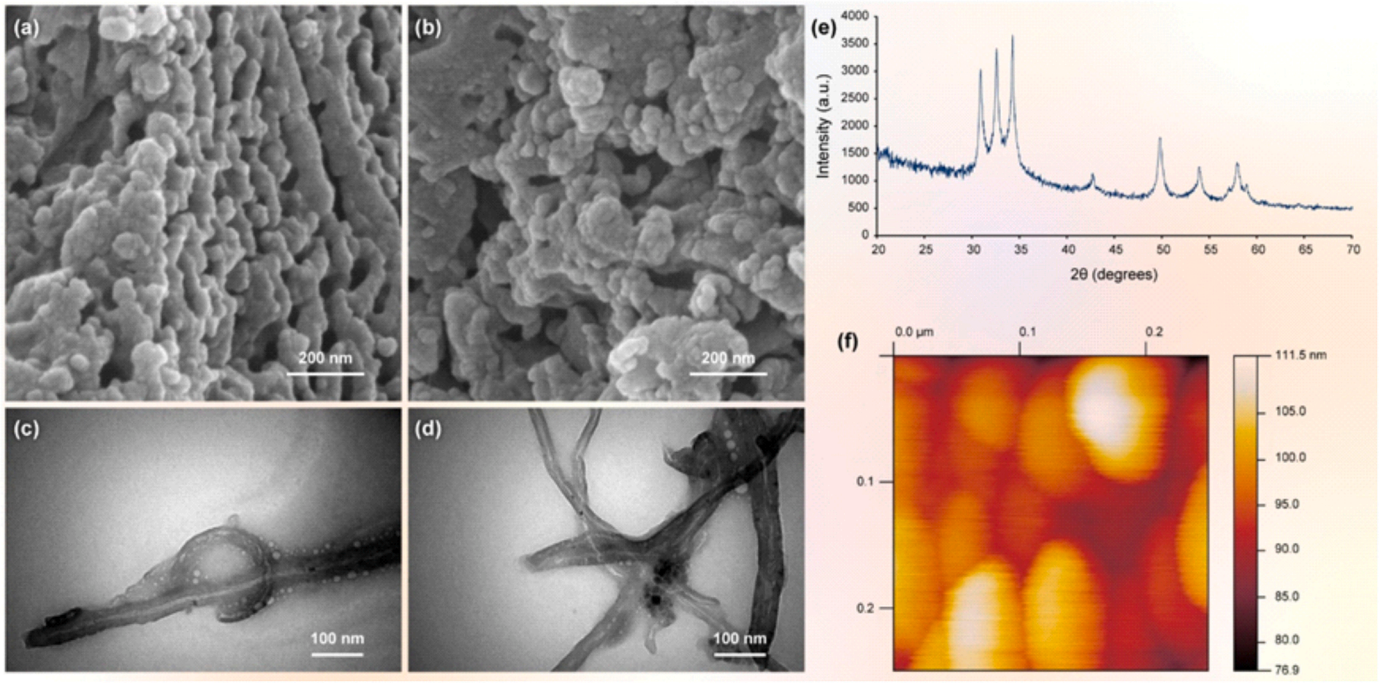

Fig. 1. FESEM (A and B), TEM (C and D), XRD (E), and AFM (F) images of the synthesized CaZnO NGs.

aggregation was observed by observing the arrays on the FESEM (Fig. 1a and b); however, based on our prior experience, more aggregations were expected in the presence of *Rosmarinus officinalis*. Therefore, it has been concluded that the leaf extract constituents not only could serve as a stabilizing agent (Akhavan et al., 2012b) but, being crystallizable inside the structure of the synthesized NGs, can reduce the aggregations and mimic the predictable array of the previous corroborating report (Akhavan et al., 2014). This is the first time observation for a leaf extract's effect on the crystallization of an inorganic nanostructure. Therefore, the exact mechanism is unknown, and only the observations are reported in this work.

The TEM images (Fig. 1c and d) showed that the NGs structures bear a resemblance to the nature-inspired NGs extracted from the living cells, thus affirming the conceptual synthesis of the first fully inorganic NG equivalent. In addition, the rode-like structure of these NGs is in good agreement with the predictable arrays on the FESEM. Again, these images confirmed the hypothesis of mimicking the MSCs structures using fully inorganic nanostructure, but with superior and modifiable features, which will be presented later.

In order to prove the crystallinity and the exact structure of the CaZnO NGs, a PXRD analysis was conducted. Based on the results (Fig. 1e), the 2θ degrees related to the presence of ZnO and Ca on the structure and attributed to the (101), (100), (102), (110), (002), (103), and (112) planes of the ZnO composition (Rabiee et al., 2020b). In addition, some of the diffraction patterns were broadened due to the presence of calcium and leaf extract (Kiani et al., 2020a).

Next, the AFM study was conducted to ensure the surface morphology of the synthesized NGs, nano-arrays with the roughness in the range of 12.98 nm–38.54 nm, with a predictable pattern were discerned. All these corroborating results showed a nano-array and maybe hollow structure (due to the presence of leaf extract in the crystallization process). One of the important parameters regarding using different nanomaterials for biomedical applications is their ability to interact with the cells/nuclei positively and inhibit negative interactions with the cells/nuclei and/or tissues.

The MSCs-based NGs could move inside the tissues/organs and/or cells without any negative interactions; therefore, the inorganic-based NGs have at least non-negative interactions. Also, one of the modifiable features of the synthesized NGs compared to the MSCs is their activity toward different pathogens, bacteria, and viruses. Therefore, investigating the possible interactions and their effect on destroying those biological threats is of great importance. Antibacterial activity of the synthesized NGs was investigated against two different colonies of *Bacillus cereus* and *Pseudomonas aeruginosa* (Fig. 2) to determine the positive interactions with the cells, and the results showed considerable antibacterial activity compared to the used leaf extracts. It should be noted that this positive interaction with the bacterial strains makes them suitable for potential biomedical applications both *in vitro* and *in vivo*. It was previously shown that nanomaterials could show antibacterial effects through the following known mechanisms: generation of reactive oxygen species by the nanomaterials during the respiration/metabolic activity of bacteria (Akhavan and Ghaderi, 2012; Rabiee et al., 2020d, 2021d), catalytic charge transferring (Akhavan and Ghaderi, 2009), metallic ion release (Akhavan, 2009; Nikfarjam et al., 2021; Truong et al., 2021), wrapping/trapping the bacteria within the aggregated nanomaterials (Akhavan et al., 2011; Rabiee et al., 2020e), membrane disruption by the extremely sharp edges of nanomaterials (Akhavan and Ghaderi, 2010), DNA/RNA damaging (Akhavan et al., 2013a), and nanobubble generation and explosion (Jannesari et al., 2020).

In this work, the antibacterial activity of the CaZnO-based NGs can be ascribed to their sharp edges (visible in TEM images) and their aggregation (observable in SEM images), their potential capability for the metal oxide-based catalytic reactions, and also Zn ion release.

In view of the presence of porphyrin on the surface of the CaZnO-based NGs, a significant fluorescence effect was expected (Rabiee et al., 2020h), which was evaluated with hydrogen peroxide. This reactant leads to the deformation of the porphyrin nanostructure and decay in the fluorescence emission spectra. The changes were considered in the range of 0–200 µM of hydrogen peroxide (Fig. 3A), thus enabling them for appropriate biosensor applications.

One of the significant challenges in bioinorganic chemistry is the safer synthesis and generation of biocompatible nanostructures (Akhavan et al., 2012a, 2015, 2016a). Hence, these CaZnO-based NGs were evaluated by MTT assay on the HEK-293, HeLa, HepG2, and PC12 cell lines after 24 h of treatment (Figs. 3B), 48 (Fig. 3C), and 72 (Fig. 3D); all cell viability results indicate that the CaZnO-based NGs have suitable

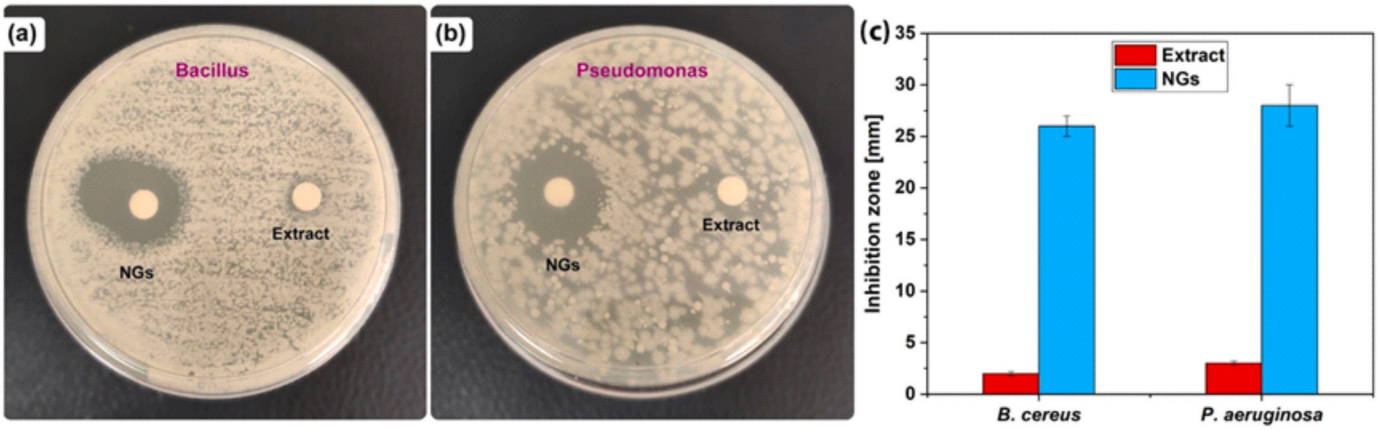

Fig. 2. Antibacterial activity of the synthesized NGs compared to the leaf extracts against (a) *Bacillus cereus* and (b) *Pseudomonas aeruginosa* bacterial strains.

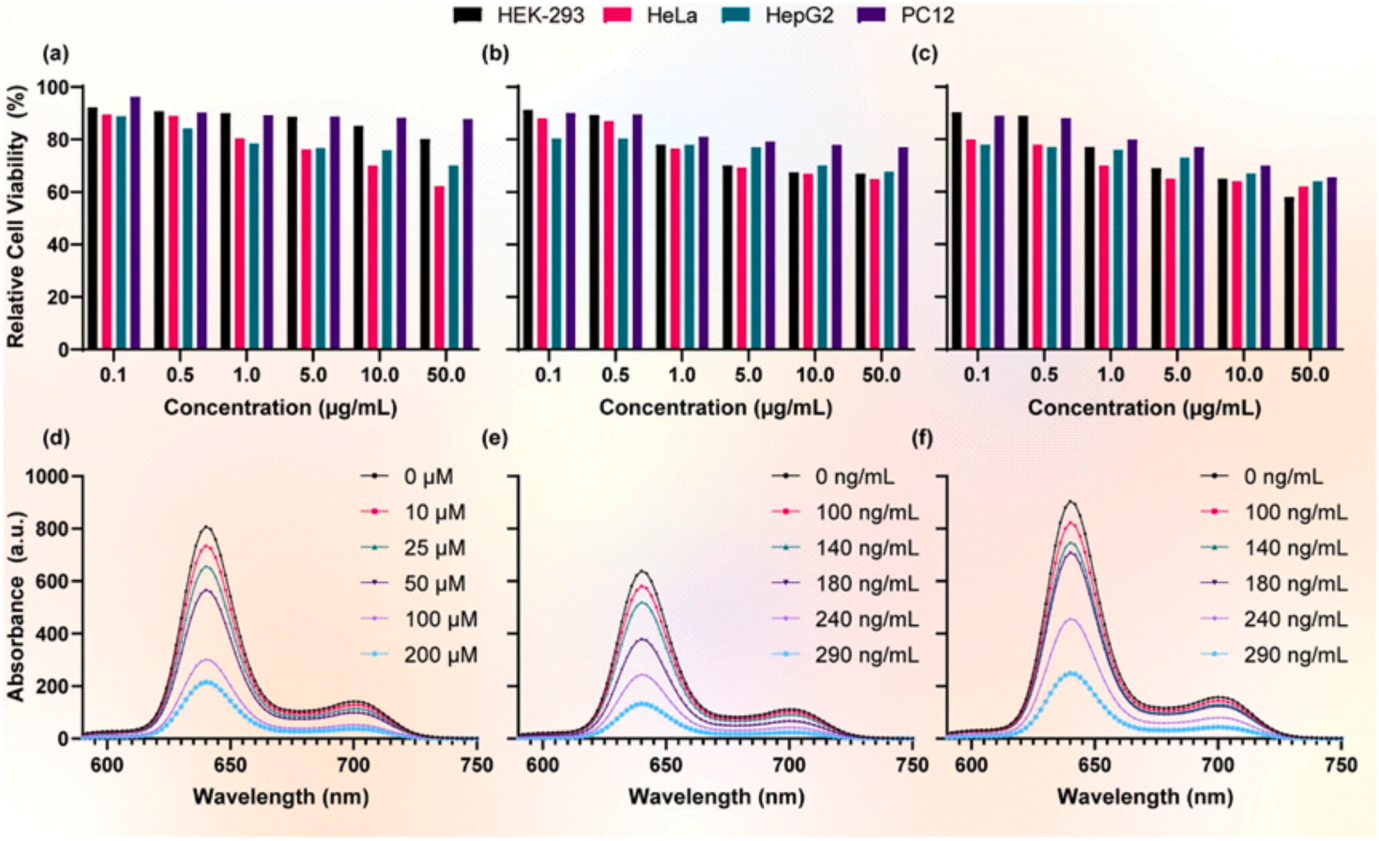

Fig. 3. (a) Relative cell viability of the synthesized NGs with different concentrations on the HEK-293, HeLa, HepG2, and PC12 cell lines after 24 h. (b), 48 h (c) and 72 h of treatment; (d) Fluorescence emission spectra of the synthesized NGs-porphyrin in the presence of different concentrations of hydrogen peroxide. (e, f) Fluorescence emission spectra of the synthesized NGs-porphyrin in the presence of different concentrations of PMA added to the HEK-293 cell line (e) and HeLa cell line (f).

cell viability on < 1 μg/mL. The higher concentrations (up to 50 μg/mL) showed minimal and controlled cytotoxicity, with the median relative cell viability of 64%. These results point toward that the synthesized NGs have acceptable biocompatibility for further biomedical appliances relative to the existing literature (Farjadian et al., 2018; Ghadiri et al., 2020). The synthesized NGs were used to detect the release of H_2O_2, which was assessed on the HEK-293 and HeLa cell lines; 12-myristate 13-acetate (PMA) was utilized as the stimulus agent to measure the H_2O_2 release. PMA can stimulate a series of signaling pathways, which results in the release of H_2O_2 from living cells in a non-controlled way.

The results showed that after the addition of 100 ng/mL of PMA, the fluorescence emission starts to decay considerably on both the HEK-293 (Fig. 3E) and HeLa (Fig. 3F) cell lines; this concentration is equivalent to the addition of 22 μM and 30 μM of hydrogen peroxide on the HEK-293 and HeLa cell lines, respectively. Further, the addition of PMA up to 290 ng/mL led to an increase in the slope of fluorescence emission decay. Therefore, it can be concluded that these modified NGs can detect low concentrations of released hydrogen peroxides from living cells.

Although the synthesis of these NGs with the assistance of 1,800 MHz fields has not revealed different structural characteristics based on the crystal structures, a considerable change in the bulk structure was observed. Thus, if we succeed in synthesizing the inorganic-based NGs,

with the same significant biological results and mimicking those from the MSCs-based NGs, the biochemical characteristics should improve by applying the high fields, thus enhancing the porosity as well as the surface morphology. Based on the FESEM images (Fig. 4A, B, C, and D), the morphology of the synthesized NGs completely changed after assembly with the assistance of 1,800 MHz; morphology changed to the hollow-nanotube structures, resembling the MSCs-based NGs.

In addition, the TEM images (Fig. 4E and F) showed very interesting morphology comprising double-aligned hollow-nanotube-like structures with a little aggregation of nanoparticles. These images confirmed the successful synthesis of fully inorganic NGs, like the MSCs-based NGs. Interestingly, the MTT assay showed higher cellular viability compared to the traditional synthesis method, and in most of the cases, after 24, 48, and 72 h of treatment, the cell viabilities were more than 90% (Fig. 4G, H and I), being similar to the MSCs-based NGs as well. The incorporation of the porphyrin on the surface of the final NGs was conducted, and the fluorescence spectra showed more homogenous and trending emissions (Fig. 3J and K); emission spectra are more homogenous and in expectable trend than the old one (before using 1,800 MHz field).

In order to analyze the pCRISPR and ssDNA interactions with the NGs, these genetic materials were exposed to varying concentrations of NGs. Quenching of the fluorescence emission of the NGs-porphyrin was expected because of the presence of similar interaction of the Zn(Ca)–O–P bonds as recently shown by Yu et al. in the presence of Zr-MOF and ssDNA (Yu et al., 2020a). The results of the fluorescence emission spectra revealed that after loading the ssDNA on the NGs-porphyrin, the fluorescence emission decayed significantly (Fig. 5A). By increasing the ratio of ssDNA to NGs-porphyrin up to 40, the fluorescence emission spectrum decayed almost wholly, indicating the successful interaction between the NGs-porphyrin and the ssDNA. However, by doing this experiment with the pCRISPR, the fluorescence emission spectra did not show a significant decrease (Fig. 5B), presumably due to the lack of O–P bonds on the surface of the pCRISPR. The surface morphology of the fully quenched NGs-porphyrin showed little tubular structure for the ssDNA (Fig. 5C and D); however, these cleared after loading of the pCRISPR (Fig. 5E and F). This may be because of the size and surface morphology of the pCRISPR, which could cover the NGs completely.

TEM analysis confirmed our hypothesis and revealed that there are more tubular and NGs structures for the ssDNA than the pCRISPR (Fig. 5G–J). Notably, these unprecedented results will open a promising and novel avenue in chemistry, materials science, and biotechnology.

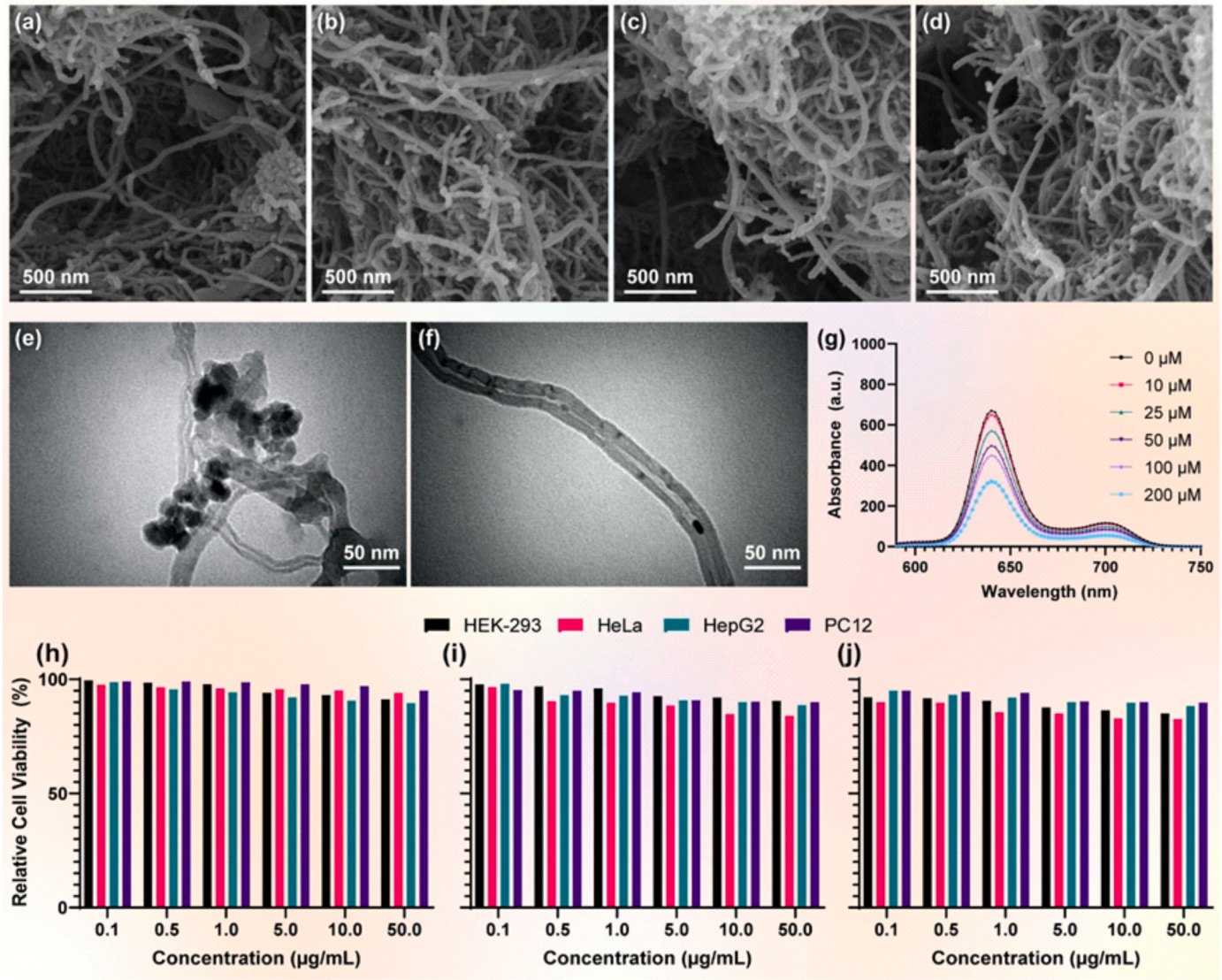

Fig. 4. FESEM (a–d), TEM (e and f), Relative cell viability of the synthesized NGs in assistance of 1,800 MHz field with different concentrations on the HEK-293, HeLa, HepG2, and PC12 cell lines after 24 h (h), 48 h (i) and 72 h (j) of treatment, Fluorescence emission spectra of the synthesized NGs-porphyrin in assistance of 1,800 MHz field with different concentrations of H_2O_2 (g).

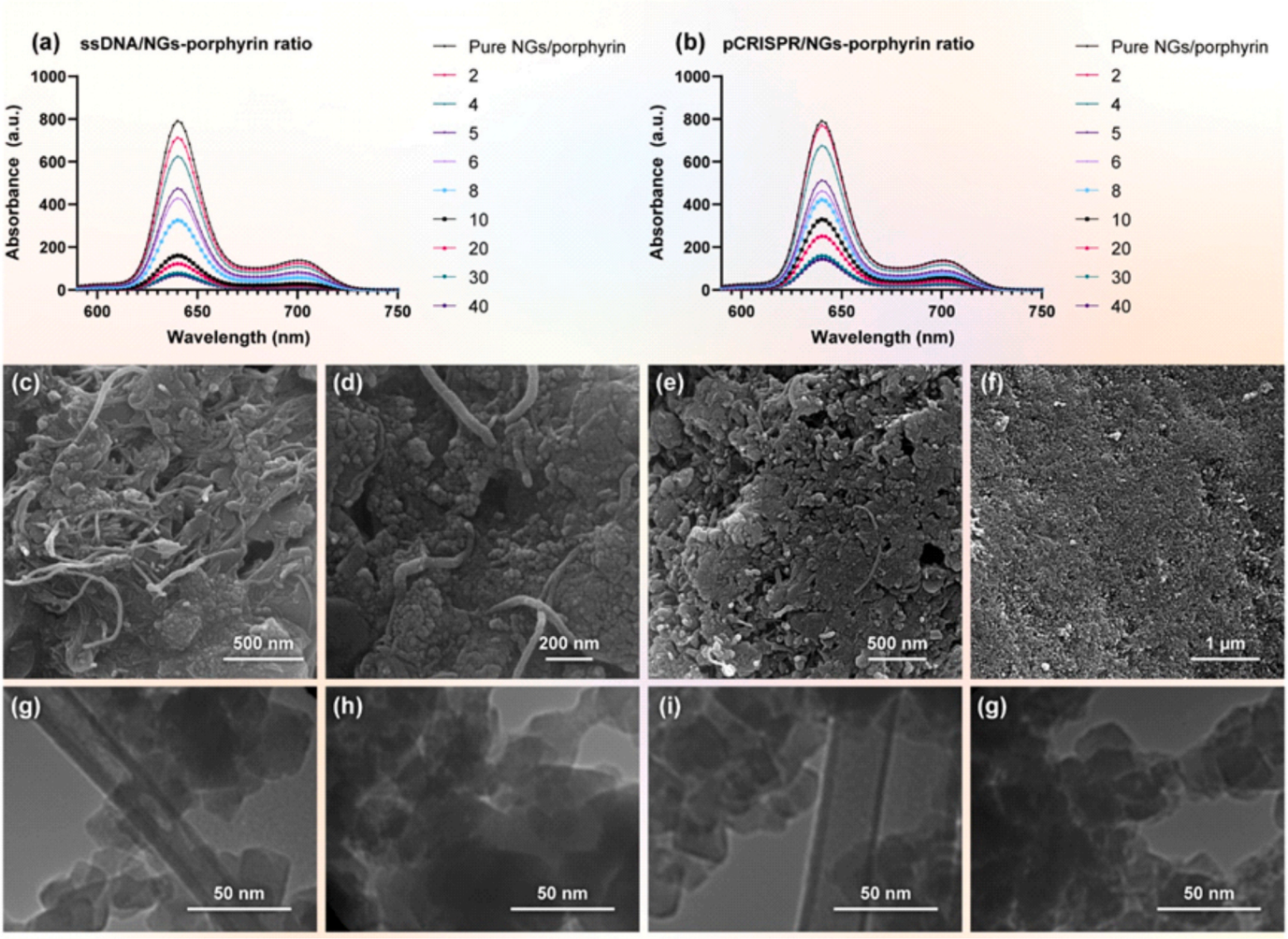

Fig. 5. Fluorescence emission spectra of the synthesized NGs-porphyrin with the assistance of a 1,800 MHz field in the presence of different concentration ratios of ssDNA (A) and pCRISPR (B). FESEM images of the synthesized NGs-porphyrin after full fluorescence decay in the presence of ssDNA (C and D) and pCRISPR (E and F). TEM images of the synthesized NGs-porphyrin after full fluorescence decay in the presence of ssDNA (G and H) and pCRISPR (I and J). The scale bars for the TEM images are 50 nm.

One of the most critical points is to identify and evaluate the presence of different concentrations of viral biomarkers (Rabiee et al., 2021a, 2021b; Rabiee et al., 2021e). Today, the most critical challenge for humanity is the identification of varying concentrations of coronavirus biomarkers, and of the utmost importance is the optical detection methods for the surface spike proteins (Rabiee et al., 2020c; Rabiee et al., 2020g; Ahmadi et al., 2021). Identifying these surface proteins can help prevent unwanted virus mutations and spread. Therefore, in this study, the ability of synthesized NGs to identify and evaluate the spike protein antigen was considered.

The results showed that (Fig. 6) by increasing the RSCSA concentration up to 10, the predictable and linear slope of the fluorescence decay could be observed, which affirms the successful optical detection of the SARS-CoV-2 spike antigen. However, by increasing the concentration to higher than 50, the slope increased considerably, and the fluorescence spectra quenched significantly, which could be used to detect the high concentrations of the SARS-CoV-2 spike antigen. The results showed that the NGs-based probes could detect the trace concentrations of the SARS-CoV-2 spike antigen with the limit of detection being 10 nM. Interestingly, after the full fluorescence decay procedure, TEM was conducted to examine the morphology of the NGs. The results showed that the NGs appeared almost with full coverage of the microenvironments and/or spike antigens; however, the rode-like morphology of the NGs remained intact. The size of the rode-like NGs decreased after the treatment with the SARS-CoV-2 spike antigen due to the electron transfers between the spike antigen, porphyrin ring, and the CaZnO-based NGs, which led to chemical oxidation of the NGs and thus reducing their size. Therefore, the electron transfer mechanisms were accelerated by decorating the surface of the NGs-porphyrin with the SARS-CoV-2 spike antigen, which led to the formation of nano-size NGs compared to the original form.

The synthesized NGs under variable conditions, including the synthesis with the assistance of 1,800 MHz, and the functionalized NGs with porphyrin were used to examine the ability of drug loading, internalization, and biocompatibility with the HT-29 cell line. In this regard, bright-field, Gray-scale, DAPI stained, DOX, and merged images have been acquired (Fig. 7), revealing promising results; unmodified and newly synthesized NGs exhibited superior drug internalization inside HT-29 cells with promising results at the minimum concentration based on the literature. After changing the synthesis system (from the normal method to using 1,800 MHz), it appears that the HT-29 cells were isolated from each other, which would be because of the presence of more rode-like NGs and their sizes. After treatment with porphyrin, the resolution of internalization of DOX increased, which is a normal phenomenon because of the optical ability of porphyrin to the cells and its fluorescence effect by itself. The drug loading capacity for the NGs, NGs with the assistance of 1,800 MHz, and NGs-porphyrin was calculated at about 59.2, 55.8, and 61.2%, respectively.

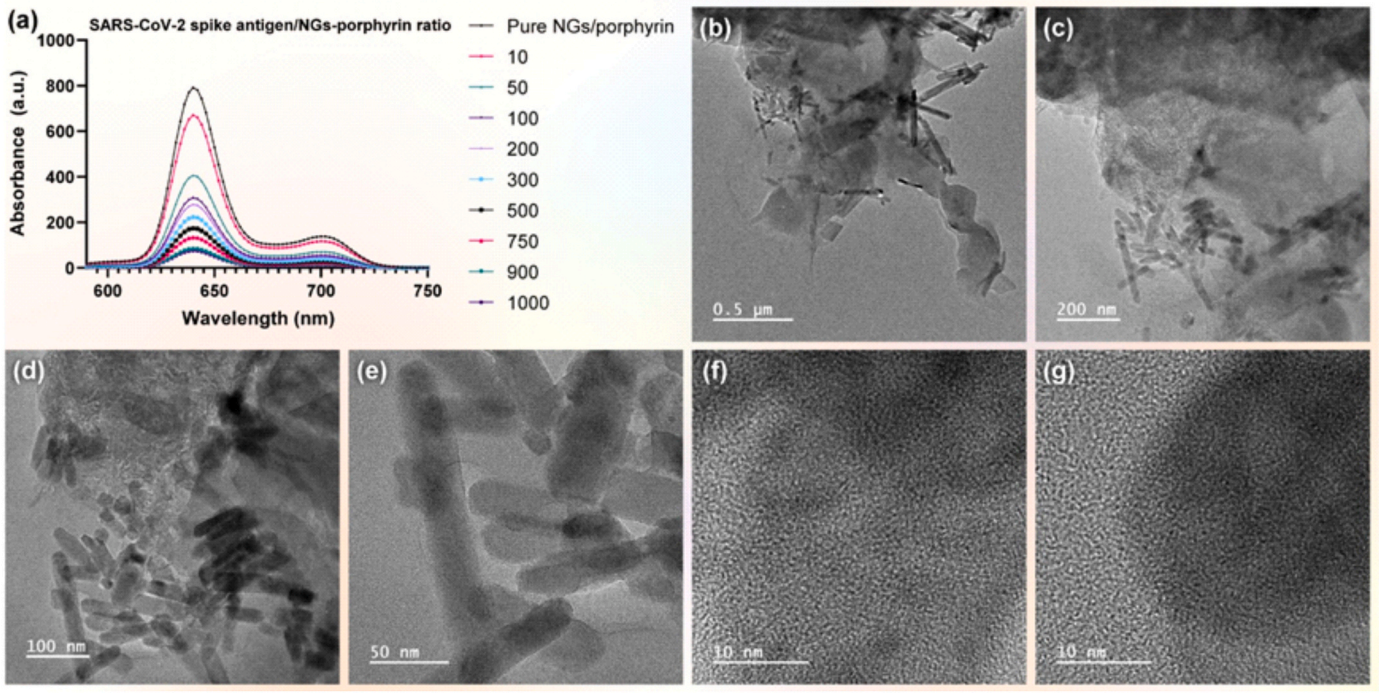

Fig. 6. Fluorescence emission spectra of the synthesized NGs-porphyrin with the assistance of 1,800 MHz field in the presence of different concentration ratios of recombinant SARS-CoV-2 spike antigen (a). TEM images of the synthesized NGs-porphyrin after fully fluorescence decay in the presence of recombinant SARS-CoV-2 spike antigen (b–g).

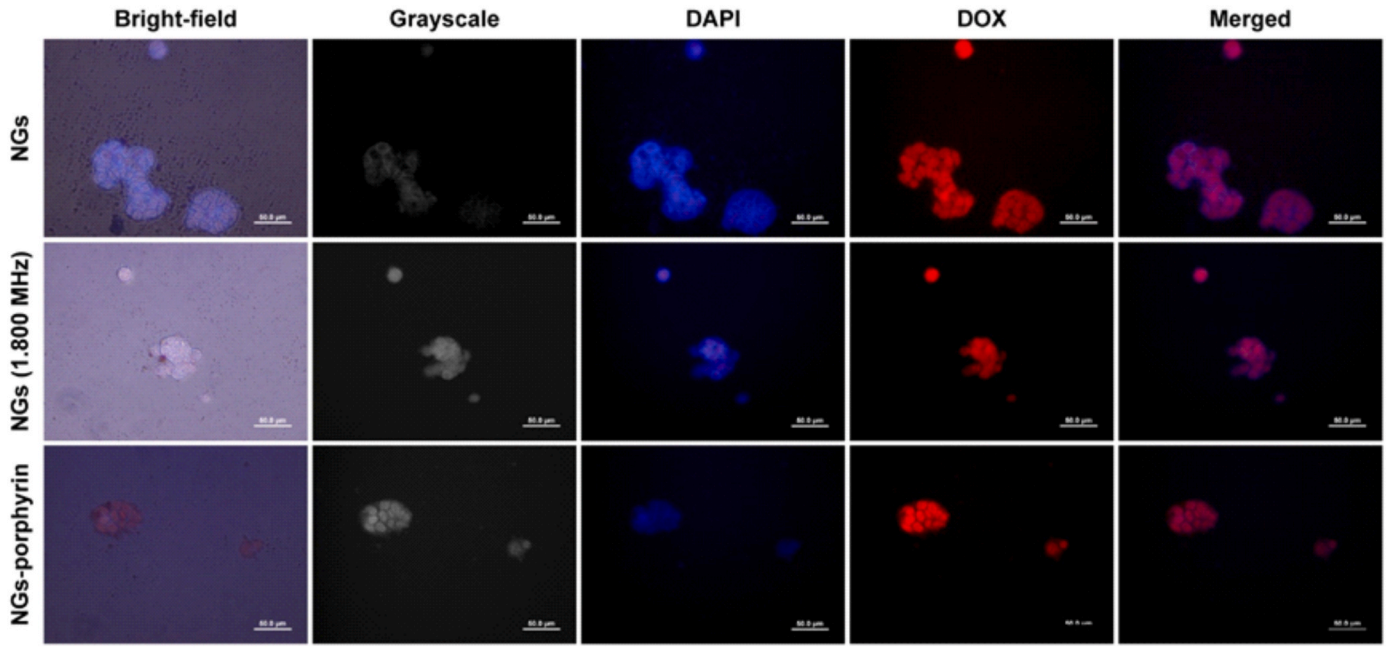

Fig. 7. CLSM images of the HT-29 cells treated with the NGs (A, B, C, D, and E), NGs in assistance of 1,800 MHz field (F, G, H, I, and J) and also NGs-porphyrin (K, L, M, N, and O). Bright-field (A, F, and K), Gray-scale (B, G, and L), DAPI stained (C, H, and M), DOX (D, I, and N), and merged (E, J, and O) images.

In contrast to the existing literature (Hui et al., 2019; Yu et al., 2020b; Saeb et al., 2021), this is the first report of an inorganic nanomaterial secured without any purification, which is endowed with the drug loading capacity and the incredible internalizations into the HT-29 cells. Some research groups have reported the critical parameters regarding the tunability of the nano-carriers before any transfections and internalizations (Vivero-Escoto et al., 2009; Du et al., 2011; Manzano and Vallet-Regí, 2020). However, the merit of this study resides in the synthesis that precludes any extensive purifications and the generation of fully compatible nanostructures to the biological matrix. All the results and concluding remarks are presented in Fig. 8. One of the key advantages of these NGs is their non-contact interactions with the cells/tissues/organs, which is a considerable advantage compared to other types of inorganic nanomaterials, including metal-organic frameworks (MOFs). A wide range of MOFs have been used for different biomedical applications (Table 1). However, none of them had the ability such as

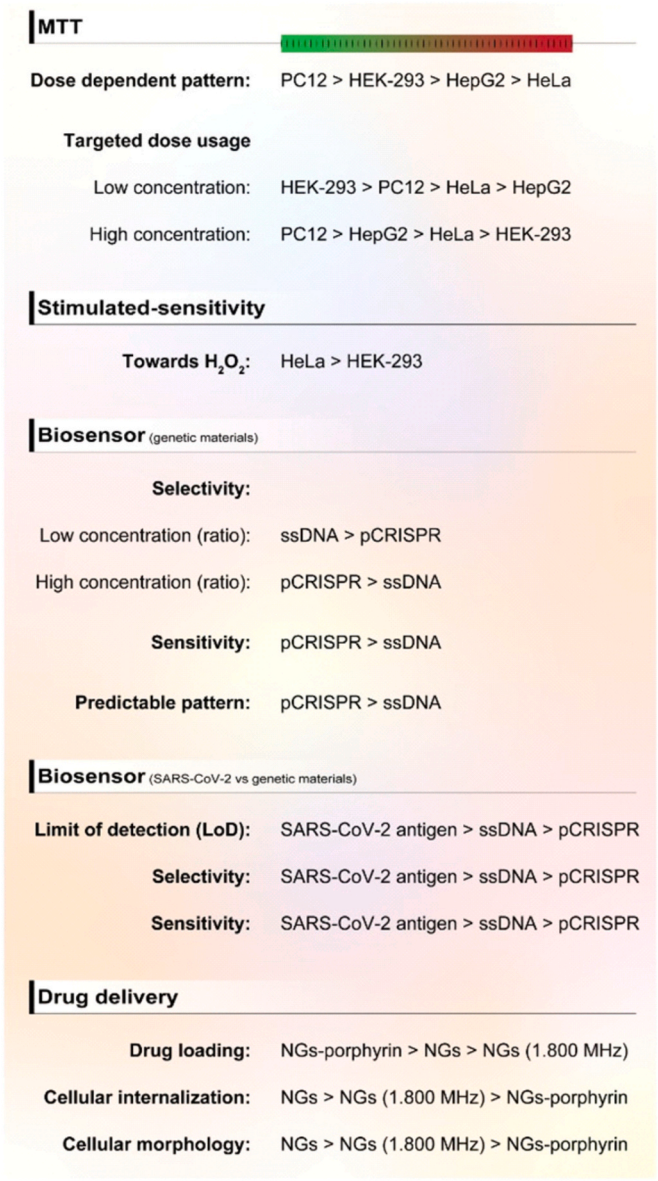

Fig. 8. A summary of the results from this study.

these NGs.

4. Conclusion

In this work, the CaZnO-based NGs were synthesized via a novel procedure using a high-gravity technique and a 1,800 MHz field while utilizing the leaf extract of *Rosmarinus officinalis* as a green template agent. Thorough chemical, physical and biological investigations have revealed that the synthesized NGs have comparable features to the MSCs NGs; these NGs showed excellent and unprecedented biocompatibility and superb ability for interaction with ssDNA- and/or pCRISPR-surface and features resembling the MSCs NGs, as revealed by morphological analysis. Furthermore, these inorganic NGs' sensing/folding ability of ssDNA and pCRISPR, along with the *in-situ* hydrogen peroxide detection on the HEK-293 and HeLa cell lines, was found to be promising, which may lead to further explorations in this nascent area.

In other experiments, the decorated NGs' ability to detect low concentrations of RSCSA (with the detection limit of 10 nM) was explored, and the predictable/linear trends of the early detection of the spike antigen could be concluded. Furthermore, the porous NGs' ability to encapsulate drug and their internalization in the HT-29 cell line revealed similar behavior compared to the MSCs in the cellular microenvironments. Therefore, it could be possible to classify the CaZnO-based nanomaterials that have been synthesized with the assistance of 1,800 MHz being the same as the MSCs structures.

These fully synthesized NGs could increase the application of MSCs-like structures in different fields, including drug delivery, gene delivery, tissue engineering, biosensors, and even industrial applications, including catalytic and photocatalytic applications. Furthermore, because of the non-contact ability of the synthesized NGs to any of the organs/tissues/cells, they could be deployed in targeted (bio)sensors without using any types of biomarkers. However, the effect of these types of nanomaterials in biological systems should be investigated in more detail in the future.

Table 1
A comparison between the inorganic NGs and MOFs for multifunctional biomedical applications.

The (nano) material	Application	Key advantageous	Ref.
UiO-66-NH_2 MOF	Co-delivery of DOX/pCRISPR	High transfection of pCRISPR, High drug loading	(Rabiee et al., 2021b; Ahmadi et al., 2022)
MOF-5	Delivery of a wide range of molecules/drugs	High loading ability	Rabiee et al., (2021c)
MOF-5	(bio)senensor of coronavirus	High surface modification ability, highly sensitive to coronavirus	Rabiee et al., (2022)
ZIF-8	Tissue engineering, drug delivery, (bio)sensor	Considerable loading ability, tunable surface functional groups	Velásquez-Hernández et al., (2021)
ZIF-67	Drug delivery, (bio)sensor	Stimuli-responsive behavior, tunable pore size	Wu et al., (2021)
CaZnO-based NGs	Drug delivery, (bio)sensor	It does not have any interaction with the cells/tissues/organs	This work

CrediT author Statement

Navid Rabiee: Conceptualization, Data curation, Investigation, Methodology, Software, Writing- original draft, Supervision. **Omid Akhavan**: Funding acquisition, Project administration, Validation. **Yousef Fatahi**: Visualization, Writing- original draft. **Amir Mohammad Ghadiri**: Methodology, Software. **Mahsa Kiani**: Methodology, Software. **Mohammad Reza Saeb**: Writing- original draft, Validation. **Pooyan Makvandi**: Writing- original draft, Validation. **Mohammad Rabiee**: Conceptualization, Supervision, review & editing the manuscript. **Mohammad Hossein Nicknam**: Review & editing the manuscript. **Rajender S. Varma**: Conceptualization, Supervision, review & editing the manuscript. **Milad Ashrafizadeh**: Writing – original draft, Methodology. **Ehsan Nazarzadeh Zare**: Supervision, review & editing the manuscript. **Esmaeel Sharifi**, Supervision, review & editing the manuscript. **Eder C. Lima**, Supervision, review & editing the manuscript.

Declaration of competing interest

The authors declare that they have no known competing financial interests or personal relationships that could have appeared to influence the work reported in this paper.

Data availability

No data was used for the research described in the article.

Acknowledgments

E.C. Lima thanked CNPq (Conselho Nacional de Desenvolvimento Científico e Tecnológico), CAPES (Coordenação de Aperfeiçoamento de Pessoal de Nível Superior), and FAPERGS (Fundação de Amparo à Pesquisa do Estado do Rio Grande do Sul) for financial support and fellowships.

Appendix A. Supplementary data

Supplementary data to this article can be found online at https://doi.org/10.1016/j.chemosphere.2022.135578.

References

Ahmadi, S., Jajarmi, V., Ashrafizadeh, M., Zarrabi, A., Haponiuk, J.T., Saeb, M.R., Lima, E.C., Rabiee, M., Rabiee, N., 2022. Mission impossible for cellular internalization: when porphyrin alliance with UiO-66-NH2 MOF gives the cell lines a ride. J. Hazard Mater. 129259.

Ahmadi, S., Rabiee, N., Bagherzadeh, M., Elmi, F., Fatahi, Y., Farjadian, F., Baheiraei, N., Nasseri, B., Rabiee, M., Dastjerd, N.T., 2020. Stimulus-responsive sequential release systems for drug and gene delivery. Nano Today 34, 100914.

Ahmadi, S., Rabiee, N., Fatahi, Y., Hooshmand, S.E., Bagherzadeh, M., Rabiee, M., Jajarmi, V., Dinarvand, R., Habibzadeh, S., Saeb, M.R., 2021. Green chemistry and coronavirus. Sustain. Chem. Pharm. 100415.

Akhavan, O., 2009. Lasting antibacterial activities of Ag–TiO2/Ag/a-TiO2 nanocomposite thin-film photocatalysts under solar light irradiation. J. Colloid Interface Sci. 336, 117–124.

Akhavan, O., 2010. Graphene nanomesh by ZnO nanorod photocatalysts. ACS Nano 4, 4174–4180.

Akhavan, O., Ghaderi, E., 2009. Photocatalytic reduction of graphene oxide nanosheets on TiO2 thin film for photoinactivation of bacteria in solar light irradiation. J. Phys. Chem. C 113, 20214–20220.

Akhavan, O., Ghaderi, E., 2010. Toxicity of graphene and graphene oxide nanowalls against bacteria. ACS Nano 4, 5731–5736.

Akhavan, O., Ghaderi, E., 2012. Escherichia coli bacteria reduce graphene oxide to bactericidal graphene in a self-limiting manner. Carbon 50, 1853–1860.

Akhavan, O., Ghaderi, E., Abouei, E., Hatamie, S., Ghasemi, E., 2014. Accelerated differentiation of neural stem cells into neurons on ginseng-reduced graphene oxide sheets. Carbon 66, 395–406.

Akhavan, O., Ghaderi, E., Akhavan, A., 2012a. Size-dependent genotoxicity of graphene nanoplatelets in human stem cells. Biomaterials 33, 8017–8025.

Akhavan, O., Ghaderi, E., Emamy, H., Akhavan, F., 2013a. Genotoxicity of graphene nanoribbons in human mesenchymal stem cells. Carbon 54, 419–431.

Akhavan, O., Ghaderi, E., Esfandiar, A., 2011. Wrapping bacteria by graphene nanosheets for isolation from the environment, reactivation by sonication, and inactivation by near-infrared irradiation. J. Phys. Chem. B 115, 6279–6288.

Akhavan, O., Ghaderi, E., Hashemi, E., Akbari, E., 2015. Dose-dependent effects of nanoscale graphene oxide on reproduction capability of mammals. Carbon 95, 309–317.

Akhavan, O., Ghaderi, E., Shahsavar, M., 2013b. Graphene nanogrids for selective and fast osteogenic differentiation of human mesenchymal stem cells. Carbon 59, 200–211.

Akhavan, O., Hashemi, E., Zare, H., Shamsara, M., Taghavinia, N., Heidari, F., 2016a. Influence of heavy nanocrystals on spermatozoa and fertility of mammals. Mater. Sci. Eng. C 69, 52–59.

Akhavan, O., Kalaee, M., Alavi, Z., Ghiasi, S., Esfandiar, A., 2012b. Increasing the antioxidant activity of green tea polyphenols in the presence of iron for the reduction of graphene oxide. Carbon 50, 3015–3025.

Akhavan, O., Saadati, M., Jannesari, M., 2016b. Graphene jet nanomotors in remote-controllable self-propulsion swimmers in pure water. Nano Lett. 16, 5619–5630.

Akça, A., Karaman, O., Karaman, C., 2021. Mechanistic insights into the catalytic reduction of N_2O by CO over Cu-embedded graphene: a density functional theory perspective. ECS J. Solid State Sci. Technol. 10, 041003.

Bagherzadeh, M., Rabiee, N., Fatahi, Y., Dinarvand, R., 2021. Zn-rich (GaN) 1− x (ZnO) x: a biomedical friend? New J. Chem. 45, 4077–4089.

Brown, S., 2013. Cancer gets spooked. Nat. Nanotechnol. 1-1.

Deng, C., Seidi, F., Yong, Q., Jin, X., Li, C., Zhang, X., Han, J., Liu, Y., Huang, Y., Wang, Y., 2022. Antiviral/antibacterial biodegradable cellulose nonwovens as environmentally friendly and bioprotective materials with the potential to minimize microplastic pollution. J. Hazard Mater. 424, 127391.

Du, J.-Z., Du, X.-J., Mao, C.-Q., Wang, J., 2011. Tailor-made dual pH-sensitive polymer–doxorubicin nanoparticles for efficient anticancer drug delivery. J. Am. Chem. Soc. 133, 17560–17563.

Farjadian, F., Moghoofei, M., Mirkiani, S., Ghasemi, A., Rabiee, N., Hadifar, S., Beyzavi, A., Karimi, M., Hamblin, M.R., 2018. Bacterial components as naturally inspired nano-carriers for drug/gene delivery and immunization: set the bugs to work? Biotechnol. Adv. 36, 968–985.

Gerner, C., Haudek, V., Schandl, U., Bayer, E., Gundacker, N., Hutter, H.P., Mosgoeller, W., 2010. Increased protein synthesis by cells exposed to a 1,800-MHz radio-frequency mobile phone electromagnetic field, detected by proteome profiling. Int. Arch. Occup. Environ. Health 83, 691–702.

Ghadiri, A.M., Rabiee, N., Bagherzadeh, M., Kiani, M., Fatahi, Y., Di Bartolomeo, A., Dinarvand, R., Webster, T.J., 2020. Green synthesis of CuO-and Cu_2O-NPs in assistance with high-gravity: the flowering of Nanobiotechnology. Nanotechnology 31, 425101.

Huang, Y., Huang, X., Ma, M., Hu, C., Seidi, F., Yin, S., Xiao, H., 2021. Recent advances in the bacterial cellulose-derived carbon aerogels. J. Mater. Chem. C 9, 818–828.

Hui, Y., Yi, X., Hou, F., Wibowo, D., Zhang, F., Zhao, D., Gao, H., Zhao, C.-X., 2019. Role of nanoparticle mechanical properties in cancer drug delivery. ACS Nano 13, 7410–7424.

Hwang, J., Zheng, M., Wiraja, C., Cui, M., Yang, L., Xu, C., 2020. Reprogramming of macrophages with macrophage cell membrane-derived nanoghosts. Nanoscale Adv. 2, 5254–5262.

Jannesari, M., Akhavan, O., Madaah Hosseini, H.R., Bakhshi, B., 2020. Graphene/CuO2 nanoshuttles with controllable release of oxygen nanobubbles promoting interruption of bacterial respiration. ACS Appl. Mater. Interfaces 12, 35813–35825.

Kaneti, L., Bronshtein, T., Malkah Dayan, N., Kovregina, I., Letko Khait, N., Lupu-Haber, Y., Fliman, M., Schoen, B.W., Kaneti, G., Machluf, M., 2016. Nanoghosts as a novel natural nonviral gene delivery platform safely targeting multiple cancers. Nano Lett. 16, 1574–1582.

Karaman, C., 2021. Orange peel derived-nitrogen and sulfur Co-doped carbon dots: a nano-booster for enhancing ORR electrocatalytic performance of 3D graphene networks. Electroanalysis 33, 1356–1369.

Karaman, O., 2022. Three-dimensional graphene network supported nickel-cobalt bimetallic alloy nanocatalyst for hydrogen production by hydrolysis of sodium borohydride and developing of an artificial neural network modeling to forecast hydrogen production rate. Chem. Eng. Res. Des. 181, 321–330.

Kholafazad-Kordasht, H., Hasanzadeh, M., Seidi, F., 2021. Smartphone-based immunosensors as next-generation healthcare tools: technical and analytical overview towards the improvement of personalized medicine. TrAC, Trends Anal. Chem. 145, 116455.

Kiani, M., Rabiee, N., Bagherzadeh, M., Ghadiri, A.M., Fatahi, Y., Dinarvand, R., Webster, T.J., 2020a. High-gravity-assisted green synthesis of palladium nanoparticles: the flowering of nanomedicine. Nanomed. Nanotechnol. Biol. Med. 30, 102297.

Kiani, M., Rabiee, N., Bagherzadeh, M., Ghadiri, A.M., Fatahi, Y., Dinarvand, R., Webster, T.J., 2020b. Improved green biosynthesis of chitosan decorated Ag-and Co3O4-nanoparticles: a relationship between surface morphology, photocatalytic and biomedical applications. Nanomed. Nanotechnol. Biol. Med. 32, 102331.

Kordasht, H.K., Hasanzadeh, M., Seidi, F., Alizadeh, P.M., 2021. Poly (amino acids) towards sensing: recent progress and challenges. TrAC, Trends Anal. Chem. 140, 116279.

Krishnamurthy, S., Gnanasammandhan, M., Xie, C., Huang, K., Cui, M., Chan, J., 2016. Monocyte cell membrane-derived nanoghosts for targeted cancer therapy. Nanoscale 8, 6981–6985.

Liu, Y., Li, R., Liang, F., Deng, C., Seidi, F., Xiao, H., 2022. Fluorescent paper-based analytical devices for ultra-sensitive dual-type RNA detections and accurate gastric cancer screening. Biosens. Bioelectron. 197, 113781.

Lupu-Haber, Y., Bronshtein, T., Shalom-Luxenburg, H., D'Atri, D., Oieni, J., Kaneti, L., Shagan, A., Hamias, S., Amram, L., Kaneti, G., 2019. Pretreating mesenchymal stem cells with cancer conditioned-media or proinflammatory cytokines changes the tumor and immune targeting by nanoghosts derived from these cells. Advanced healthc. mater. 8, 1801589.

Manzano, M., Vallet-Regí, M., 2020. Mesoporous silica nanoparticles for drug delivery. Adv. Funct. Mater. 30, 1902634.

Mitra, S., Sasmal, H.S., Kundu, T., Kandambeth, S., Illath, K., Diaz Diaz, D., Banerjee, R., 2017. Targeted drug delivery in covalent organic nanosheets (CONs) via sequential post-synthetic modification. J. Am. Chem. Soc. 139, 4513–4520.

Mobed, A., Hasanzadeh, M., Seidi, F., 2021. Antibacterial activity of gold nanocomposites as a new nanomaterial weapon to combat photogenic agents: recent advances and challenges. RSC Adv. 11, 34688–34698.

Nikfarjam, N., Ghomi, M., Agarwal, T., Hassanpour, M., Sharifi, E., Khorsandi, D., Ali Khan, M., Rossi, F., Rossetti, A., Nazarzadeh Zare, E., 2021. Antimicrobial ionic liquid-based materials for biomedical applications. Adv. Funct. Mater. 2104148.

Nosrati, H., Seidi, F., Hosseinmirzaei, A., Mousazadeh, N., Mohammadi, A., Ghaffarlou, M., Danafar, H., Conde, J., Sharafi, A., 2022. Prodrug polymeric nanoconjugates encapsulating gold nanoparticles for enhanced X-Ray radiation therapy in breast cancer. Advanced Healthc. Mater 11, 2102321.

Rabiee, N., Bagherzadeh, M., Ghadiri, A.M., Kiani, M., Ahmadi, S., Aldhaher, A., Varma, R.S., Webster, T.J., 2020a. High-gravity-assisted green synthesis of NiO-NPs anchored on the surface of biodegradable nanobeads with potential biomedical applications. J. Biomed. Nanotechnol. 16, 520–530.

Rabiee, N., Bagherzadeh, M., Ghadiri, A.M., Kiani, M., Aldhaher, A., Ramakrishna, S., Tahriri, M., Tayebi, L., Webster, T.J., 2020b. Green synthesis of ZnO NPs via Salvia hispanica: evaluation of potential antioxidant, antibacterial, mammalian cell viability, H1N1 influenza virus inhibition, and photocatalytic activities. J. Biomed. Nanotechnol. 16, 456–466.

Rabiee, N., Bagherzadeh, M., Ghadiri, A.M., Kiani, M., Fatahi, Y., Tavakolizadeh, M., Pourjavadi, A., Jouyandeh, M., Saeb, M.R., Mozafari, M., 2021a. Multifunctional 3D hierarchical bioactive green carbon-based nanocomposites. ACS Sustain. Chem. Eng. 9, 8706–8720.

Rabiee, N., Bagherzadeh, M., Ghasemi, A., Zare, H., Ahmadi, S., Fatahi, Y., Dinarvand, R., Rabiee, M., Ramakrishna, S., Shokouhimehr, M., 2020c. Point-of-use rapid detection of sars-cov-2: nanotechnology-enabled solutions for the COVID-19 pandemic. Int. J. Mol. Sci. 21, 5126.

Rabiee, N., Bagherzadeh, M., Heidarian Haris, M., Ghadiri, A.M., Matloubi Moghaddam, F., Fatahi, Y., Dinarvand, R., Jarahiyan, A., Ahmadi, S., Shokouhimehr, M., 2021b. Polymer-coated NH2-UiO-66 for the codelivery of DOX/pCRISPR. ACS Appl. Mater. Interfaces 13, 10796–10811.

Rabiee, N., Bagherzadeh, M., Jouyandeh, M., Zarrintaj, P., Saeb, M.R., Mozafari, M., Shokouhimehr, M., Varma, R.S., 2021c. Natural polymers decorated MOF-MXene nanocarriers for Co-delivery of doxorubicin/pCRISPR. ACS Appl. Bio Mater. 4, 5106–5121.

Rabiee, N., Bagherzadeh, M., Kiani, M., Ghadiri, A.M., 2020d. Rosmarinus officinalis directed palladium nanoparticle synthesis: investigation of potential antibacterial, anti-fungal, and Mizoroki-Heck catalytic activities. Adv. Powder Technol. 31, 1402–1411.

Rabiee, N., Bagherzadeh, M., Kiani, M., Ghadiri, A.M., Etessamifar, F., Jaberizadeh, A.H., Shakeri, A., 2020e. Biosynthesis of copper oxide nanoparticles with potential biomedical applications. Int. J. Nanomed. 15, 3983.

Rabiee, N., Bagherzadeh, M., Kiani, M., Ghadiri, A.M., Zhang, K., Jin, Z., Ramakrishna, S., Shokouhimehr, M., 2020f. High gravity-assisted green synthesis of ZnO nanoparticles via Allium ursinum: conjoining nanochemistry to neuroscience. Nano Express 1, 020025.

Rabiee, N., Fatahi, Y., Ahmadi, S., Abbariki, N., Ojaghi, A., Rabiee, M., Radmanesh, F., Dinarvand, R., Bagherzadeh, M., Mostafavi, E., 2022. Bioactive hybrid metal-organic framework (MOF)-based nanosensors for optical detection of recombinant SARS-CoV-2 spike antigen. Sci. Total Environ. 825, 153902.

Rabiee, N., Fatahi, Y., Asadnia, M., Daneshgar, H., Kiani, M., Ghadiri, A.M., Atarod, M., Mashhadzadeh, A.H., Akhavan, O., Bagherzadeh, M., 2021d. Green porous benzamide-like nanomembranes for hazardous cations detection, separation, and concentration adjustment. J. Hazard Mater. 127130.

Rabiee, N., Khatami, M., Jamalipour Soufi, G., Fatahi, Y., Iravani, S., Varma, R.S., 2021e. Diatoms with invaluable applications in nanotechnology, biotechnology, and biomedicine: recent advances. ACS Biomater. Sci. Eng.

Rabiee, N., Rabiee, M., Bagherzadeh, M., Rezaei, N., 2020g. COVID-19 and picotechnology: potential opportunities. Med. Hypotheses 144, 109917.

Rabiee, N., Yaraki, M.T., Garakani, S.M., Garakani, S.M., Ahmadi, S., Lajevardi, A., Bagherzadeh, M., Rabiee, M., Tayebi, L., Tahriri, M., 2020h. Recent advances in porphyrin-based nanocomposites for effective targeted imaging and therapy. Biomaterials 232, 119707.

Saadati, A., Hasanzadeh, M., Seidi, F., 2021. Biomedical application of hyperbranched polymers: recent Advances and challenges. TrAC, Trends Anal. Chem. 142, 116308.

Saeb, M.R., Rabiee, N., Mozafari, M., Mostafavi, E., 2021. Metal-organic frameworks-based nanomaterials for drug delivery. Materials 14, 3652.

Sardaremelli, S., Hasanzadeh, M., Seidi, F., 2021. Enzymatic recognition of hydrogen peroxide (H2O2) in human plasma samples using HRP immobilized on the surface of poly (arginine-toluidine blue)-Fe3O4 nanoparticles modified polydopamine; a novel biosensor. J. Mol. Recogn. 34, e2928.

Schuderer, J., Samaras, T., Oesch, W., Spat, D., Kuster, N., 2004. High peak SAR exposure unit with tight exposure and environmental control for in vitro experiments at 1800 MHz. IEEE Trans. Microw. Theor. Tech. 52, 2057–2066.

Seidi, F., Deng, C., Zhong, Y., Liu, Y., Huang, Y., Li, C., Xiao, H., 2021. Functionalized masks: powerful materials against COVID-19 and future pandemics. Small 17, 2102453.

Shokri, Z., Seidi, F., Saeb, M.R., Jin, Y., Li, C., Xiao, H., 2022. Elucidating the impact of enzymatic modifications on the structure, properties, and applications of cellulose, chitosan, starch, and their derivatives: a review. Mater. Today Chem. 24, 100780.

Teplensky, M.H., Fantham, M., Li, P., Wang, T.C., Mehta, J.P., Young, L.J., Moghadam, P. Z., Hupp, J.T., Farha, O.K., Kaminski, C.F., 2017. Temperature treatment of highly porous zirconium-containing metal-organic frameworks extends drug delivery release. J. Am. Chem. Soc. 139, 7522–7532.

Toledano Furman, N.E., Lupu-Haber, Y., Bronshtein, T., Kaneti, L., Letko, N., Weinstein, E., Baruch, L., Machluf, M., 2013. Reconstructed stem cell nanoghosts: a natural tumor-targeting platform. Nano Lett. 13, 3248–3255.

Truong, L.B., Medina-Cruz, D., Mostafavi, E., Rabiee, N., 2021. Selenium nanomaterials to combat antimicrobial resistance. Molecules 26, 3611.

Velásquez-Hernández, M.d.J., Linares-Moreau, M., Astria, E., Carraro, F., Alyami, M.Z., Khashab, N.M., Sumby, C.J., Doonan, C.J., Falcaro, P., 2021. Towards applications of bioentities@ MOFs in biomedicine. Coord. Chem. Rev. 429, 213651.

Vivero-Escoto, J.L., Slowing, I.I., Wu, C.-W., Lin, V.S.-Y., 2009. Photoinduced intracellular controlled release drug delivery in human cells by gold-capped mesoporous silica nanosphere. J. Am. Chem. Soc. 131, 3462–3463.

Wu, J., Zhang, Z., Qiao, C., Yi, C., Xu, Z., Chen, T., Dai, X., 2021. Synthesis of monodisperse ZIF-67@ CuSe@ PVP nanoparticles for pH-responsive drug release and photothermal therapy. ACS Biomater. Sci. Eng. 8, 284–292.

Yu, K., Wei, T., Li, Z., Li, J., Wang, Z., Dai, Z., 2020a. Construction of molecular sensing and logic systems based on site-occupying effect-modulated MOF–DNA interaction. J. Am. Chem. Soc.

Yu, W., Liu, R., Zhou, Y., Gao, H., 2020b. Size-tunable strategies for a tumor-targeted drug delivery system. ACS Cent. Sci. 6, 100–116.